## 20.4 3D Surgical Alignment with 100µm Resolution Using Magnetic-Field Gradient-Based Localization

Saransh Sharma, Grace Ding, Aditya Telikicherla, Fatemeh Aghlmand, Arian Hashemi Talkhooncheh, Minwo Wang, Mikhail G. Shapiro, Azita Emami

California Institute of Technology, Pasadena, CA

Substantial advances in the field of surgery have taken place in recent years, which aim at decreasing patient morbidity through innovations in endoscopy, optical imaging, laparoscopic and robotic technologies. However, real-time imaging and navigation during high precision surgery necessitates the use of X-Ray fluoroscopy with most existing technologies to achieve precise localization. Intramedullary (IM) nailing is a common example of such high precision orthopedic surgery, which requires insertion of a nail into the medullary canal of a fractured bone followed by locking screws [1]. Proximal screw locking is performed using a mechanical guide, which is not possible for distal locking owing to the deformation (≈15mm) caused during insertion [2]. Freehand technique is typically used to localize distal holes, in which the surgical drill is aligned with the hole axis through fluoroscopic imaging. This process is time-consuming and exposes the patient and surgical team to high ionizing radiation. Various other methods, which reduce or eliminate irradiation during distal locking, are not widely used. This is attributed to their lack of compensation for significant deformation of the nail, added requirements such as computing systems, extra robotic arms, CT images, sophisticated hardware and software that require training for the surgeon and staff.

This paper presents a navigation system for 3D localization using magnetic field gradients, which is inspired by Magnetic Resonance Imaging (MRI) but does not require the strong magnetic field used in MRI [3], and can replace fluoroscopy during IM nailing. The goal is to generate monotonically varying magnetic fields in the desired Field-of-View (FOV) such that each spatial point corresponds to a unique field value. The field is sensed by miniaturized devices in the FOV and communicated wirelessly to a receiver, which maps the field to spatial coordinates and displays the device location in real-time (Fig. 20.4.1). Monotonically varying magnetic fields are generated using low-cost planar electromagnet coils, placed beneath the patient's leg. A battery-less wireless device capable of measuring and transmitting the value of its local magnetic field, is attached to the distal end of the implanted nail. This device consists of a 3D magnetic sensor (AK09970N), a CMOS chip to interface with the sensor, an off-chip coil for wireless power transfer (WPT) and data communication, and off-chip capacitors for energy storage. Another similar device is installed in the surgical drill. In the measurement phase, both devices measure magnetic fields in X, Y and Z at their respective locations. A computing system decodes the spatial position of both the devices from the received magnetic field data and displays their relative locations on a monitor, which helps the surgeon to maneuver to the hole location in real-time. The resolution of magnetic field measured by the devices ($\Delta B$) and strength of the applied magnetic field gradient (G), together set the localization resolution (LR) of the system as $LR = \Delta B/G$.

The wirelessly powered CMOS chip consists of a Power Management Unit (PMU), RF Wake-Up Unit (RFW) and Data Acquisition Unit (DAU), as shown in Fig. 20.4.2. The PMU receives wireless power at 13.56MHz and the rectifier converts it to DC power with 82% voltage conversion efficiency. It uses unbalanced-biased comparators to allow operation at low input amplitudes and to minimize leakage current [4]. This unbalance is created by appropriately selecting the values of resistors R1 and R2, which were chosen to be 30kΩ and 0.5kΩ, respectively. Voltage limiters are connected to the RF inputs to clamp the voltage to 1.2V, which prevents over-stressing of the front-end transistors. The rectified DC voltage is boosted to 4× by a two-stage interleaved switched-capacitor DC-DC boost converter (Fig. 20.4.3), which achieves a voltage conversion efficiency of 96% with no-load and 65% when peak current is driven by the regulator loads. This efficiency is achieved by using non-overlapping (NOL) clocks for switching the two stages of the boost converter to significantly reduce leakage and charge-sharing losses [5]. The boosted voltage thus obtained is provided to three regulators, which produce stable supply voltages of 2.5V for the sensor, 1V for analog and 0.5V for digital circuit blocks. The sensor regulator has a 100µF external capacitor to store energy for the measurement phase, during which the sensor consumes 2mA at 2.5V for 1ms, making it the most power hungry phase in the entire operation. Reference voltages for regulators are generated from the bandgap voltage and a resistive divider (Fig. 20.4.2).

Reset and wake-up are transmitted as ASK signals on a 13.56MHz carrier to the chip. An envelope detector in RFW detects the presence of low level zero signal in the carrier and compares that to fixed signal length thresholds to generate the reset/wake-up signal. This is fed to the DAU, which triggers a measurement by the sensor after reception of a wake-up signal. The DAU consists of an I2C digital block, which provides the bi-directional data line (SDA) and uni-directional clock line (SCL) to the sensor after appropriate level shifting. Figure 20.4.3 shows the bi-directional SDA buffer, which is controlled by an enable signal (ENA) generated by the I2C block. Another digital circuit block in the DAU is the Sensor Interface, which controls the I2C block and provides the required sequence of sensor address, register address and command bits, configuration bits for the sensor and parsing of the received data stream. A 9-stage current-starved ring oscillator generates the I2C clock and is also used for generating the NOL clocks. The measured magnetic field vector is transmitted wirelessly to an external receiver through a backscatter switch.

Magnetic field gradients are generated by electromagnets made using 50/32 AWG Litz wire (Fig. 20.4.5). The Z gradient is obtained as a decaying field from the surface of a spiral coil. For X and Y gradients, two opposite winding coils carrying the same current are placed side-by-side, Y coils being orthogonal to X. All three coils are stacked concentrically to give a 1.5cm thick flat base. To generate the required gradient strength of 30mT/m in a 20×20×10 $cm^3$ FOV, the required DC currents by the X, Y and Z coils are 18A, 20A and 13A, respectively. The gradient generated for these current values is much stronger towards the coil surface and reduces to 30mT/m on the edges of FOV. In order to get a monotonic nature of the absolute field, Z coil is kept ON for all three axes gradient. This adds the required background field to the one produced by X and Y coils to offset their negative halves and result in a monotonically varying field magnitude (Fig. 20.4.5). This is crucial for obtaining unambiguous position mapping from the field magnitude. The entire FOV is pre-characterized with spatial increments of 100µm in 3D. For each position, the ambient earth's field is subtracted from the gradient field and is stored in a look-up table. A search algorithm in MATLAB uses the look-up table and outputs the nearest position coordinate for each measurement.

The prototype implantable device is assembled on an FR4 PCB measuring 10.8mm × 6.5mm. Magnetic sensor and CMOS chip are placed on the top and storage capacitors on the bottom. The chip measures 1.5mm × 1mm and is fabricated in a 65nm CMOS process (Fig. 20.4.7). WPT coils are wound along the PCB edges. For testing, the device is placed in the FOV on top of a 5cm high saline tank with the primary WPT coil below (Fig. 20.4.6). The wake-up signal is sent wirelessly to trigger data measurement by the sensor. This is synchronized with the gradient ON/OFF signal to allow high DC currents only during the measurement phase, thus minimizing heat generated by the coils. The resulting digital signals measured by the chip are shown in Fig. 20.4.4. A backscatter receiver demodulates the received data and sends it to a MATLAB code to determine the corresponding closest position. To get an absolute error of <3µT in the measured field, given 5µT RMS noise of the sensor, an ensemble of 25 measured points was averaged (Fig. 20.4.5). This gives a localization error of less than 100µm in X, Y and Z (measured from a reference point on the coils) when the applied gradient is ≥30mT/m. The averaging window can be relaxed for a lower noise sensor or higher field gradients. This prototype can measure magnetic field at the rate of 7 times per second. The sampling limitation is mainly due to the ramp-up time (≈100ms) of currents in the external gradient coils.

Compared to state-of-the-art localization techniques, this system achieves superior 3D resolution using safe magnetic field gradients (Fig. 20.4.6) and can enable various high-precision surgeries that require real-time navigation.

*Acknowledgements:*
The authors acknowledge the contributions of S. Shah, W. Kuo, H. Sheng, H. Davis, A. Patil, K.-C. Chen and N. Phoole; Muse Semiconductor for chip fabrication; NSF Grant No. 1823036, RI2 Grant No. 101170 and Heritage Medical Research Institute for funding.

*References:*

[1] W. M. Ricci et al., "Intramedullary Nailing of Femoral Shaft Fractures: Current Concepts," *JAAOS*, vol. 17, no. 5, pp. 296-305, 2009.
[2] T. Leloup et al., "A Novel Technique for Distal Locking of Intramedullary Nail Based on Two Non-constrained Fluoroscopic Images and Navigation," *IEEE Trans. Med. Imaging,* vol. 27, no. 9, pp. 1202-12, 2008.
[3] M. Monge et al., "Localization of Microscale Devices in Vivo Using Addressable Transmitters Operated as Nagnetic Spins," *Nature Biomedical Engineering,* pp. 736-744, 2017.

 978-1-7281-3205-1/20/$31.00 

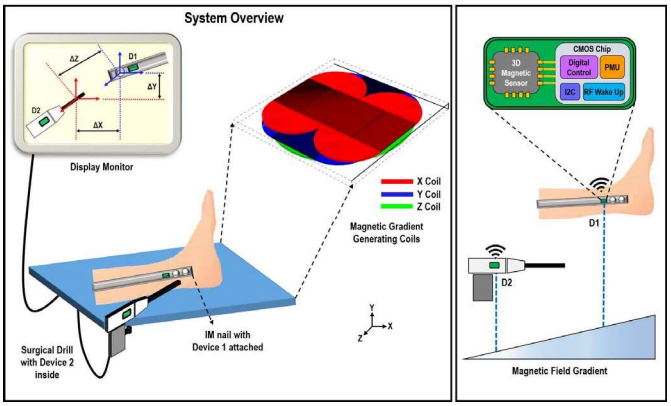


Figure 20.4.1: System overview showing the patient's leg on the top of flat magnetic gradient coils, Device 1 is on the implanted IM nail, Device 2 is installed in the surgical drill and relative positions of the two are displayed on a monitor in real-time. Working principle is shown on the right where monotonically varying magnetic field encodes each spatial point uniquely; device overview is shown on the top. This system enables navigation during surgery without using the conventional X-Ray fluoroscopy.

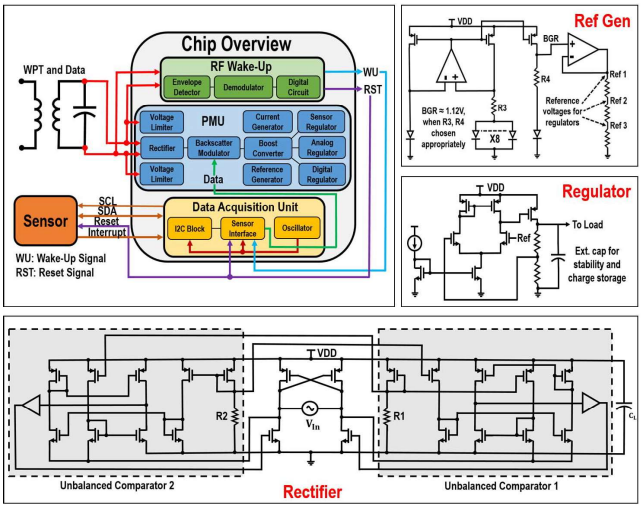


Figure 20.4.2: Chip overview (top-left); rectifier schematic (bottom) with resistors R1 (30kΩ) and R2 (0.5kΩ) for unbalanced comparators; reference generator (top-right) and regulator topology with external 100μF capacitor.

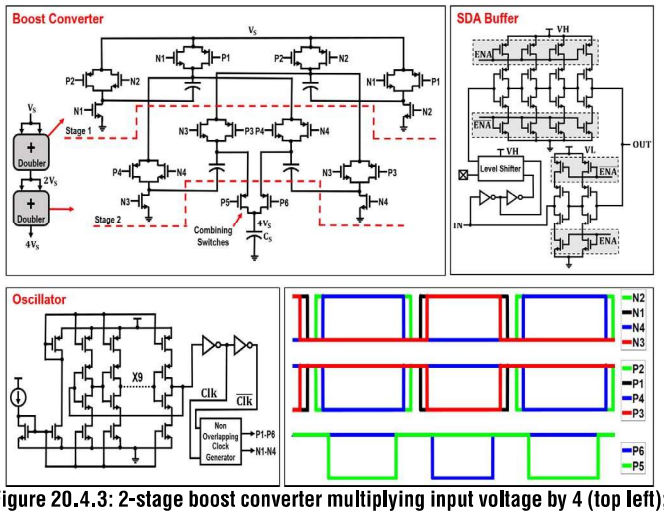


Figure 20.4.3: 2-stage boost converter multiplying input voltage by 4 (top left); oscillator schematic with NOL block (bottom-left); NOL clock waveforms (bottom-right); bi-directional SDA buffer (top-right) with input to output data flow through VH path and output to input data flow through VL path.

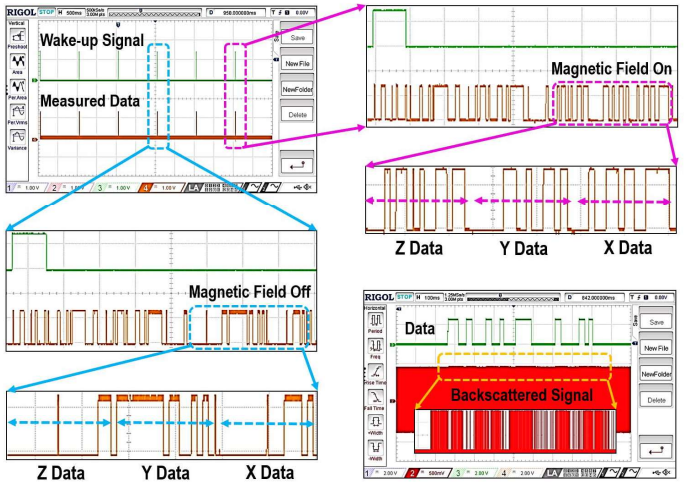


Figure 20.4.4: Measurement results for the CMOS chip: decoded wake-up signal and measured data (top-left); 16-bit data vectors for each of X, Y and Z in presence (top-right) and absence (bottom-left) of field; backscattered signal shown with much lower data speed for clarity (bottom-right).

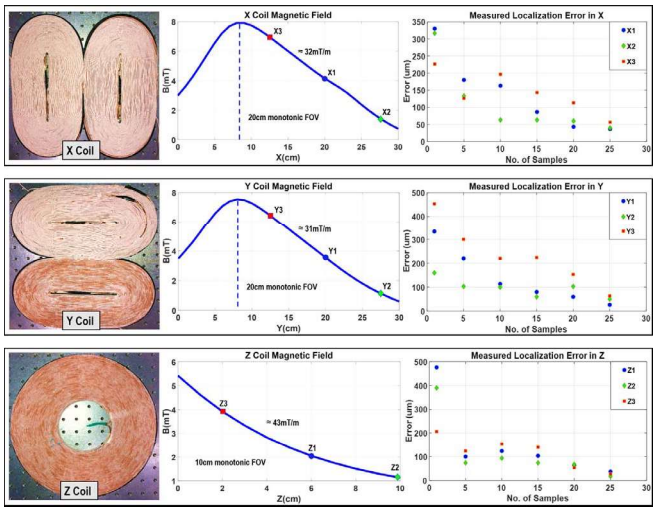


Figure 20.4.5: Gradient coils (left); magnetic field profile (middle); measured localization error (right). Averaging 25 samples gives less than 100μm localization error when measured from a fixed reference point on the coils.

| Metric | This work | Ref [3] | Ref [6] |
|---|---|---|---|
| Localization Dimension | 3D | 2D | 5D * |
| Localization Resolution | 100μm | 500μm | 2100μm |
| Localization Modality | Magnetic Field Gradient | MRI Inspired | Magnetic Field |
| Depth of Focus | 10cm | 1.2cm | 5cm |
| Sample Rate | 7Hz | NA | 200Hz |
| Field of View | 20cm x 20cm x 10cm # | 1.2cm ## | 7cm x 7cm x 5cm |
| CMOS Technology | Yes (65nm) | Yes (180nm) | No |
| Wireless Power | Yes | No | No |
| Wireless Data | Yes | Yes | No |
| Frequency | 13.56MHz | 500MHz $ | N/A |
| CMOS Chip Area | 1.5mm² | 2.16mm² | N/A |
| Avg. Power | 1mW ** | 339uW | N.R. |

* Angular orientation is also reported (3D+2D)
\# Can be enhanced by using bigger gradient coils
\## Reported for a single axis
$ Center frequency
** Includes external sensor power
N/A: Not Applicable
N.R.: Not Reported

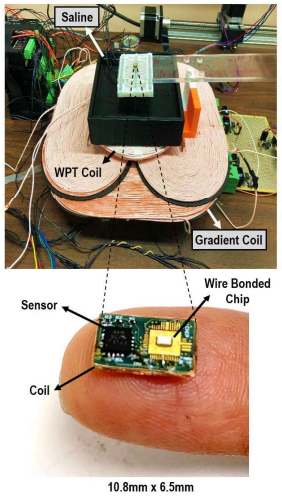


Figure 20.4.6: Comparison of the system with state-of-the-art localization techniques; in-vitro test setup (top-right); assembled prototype device (bottom-right) with storage capacitors underneath.

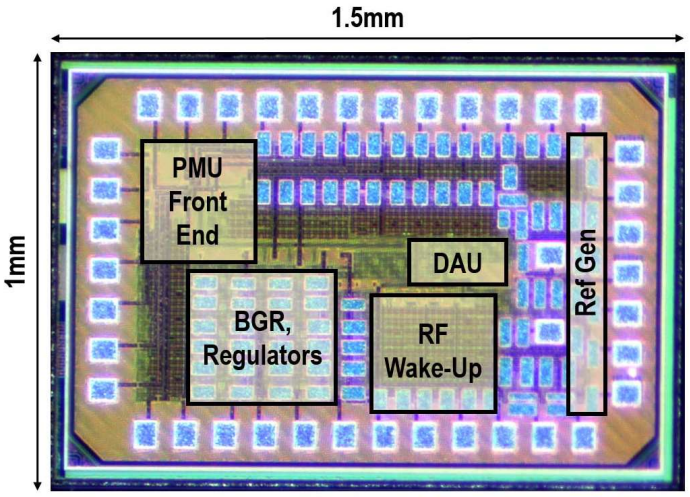


Figure 20.4.7: Micrograph of the fabricated 65nm CMOS chip.

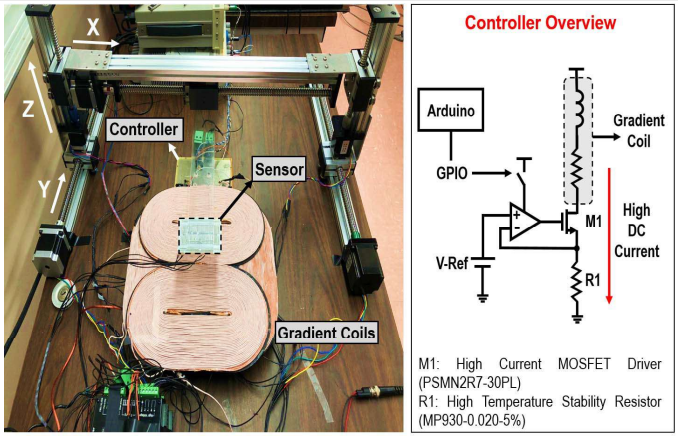


**Figure 20.4.S1: Setup for 3D characterization of gradient coils (left). Arduino is used for controlling the X, Y, Z actuators, for switching the DC current in coils and for interfacing with the sensor. Actuators move in increments of 100μm (points in between are interpolated in MATLAB) and magnetic field is measured by the sensor mounted on a fiberglass arm. Current in coils is set using a controller circuit (schematic in right) by appropriately selecting R1 and V-Ref.**

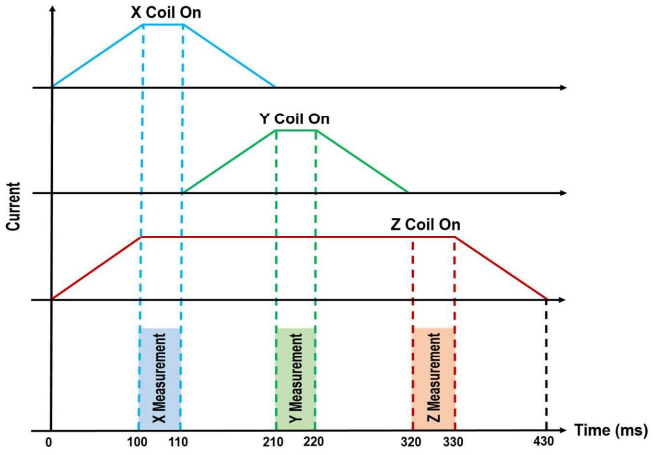


**Figure 20.4.S2: Timing diagram for coils showing their ON/OFF time window. Z coil is kept ON for the entire operation to offset the negative field values of X and Y, resulting in a monotonic field magnitude for all three dimensions. This leads to a unique field magnitude for each spatial coordinate. Measurement frequency is limited by the ramp-up time of DC current in the coils.**

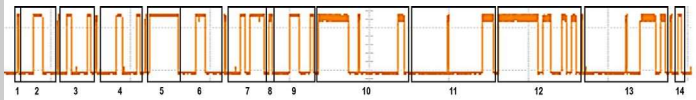


1. Start condition.
2. Sensor address (0001100) with write mode bit (0): 00011000. This allows values to be written on SDA by the chip.
3. Control register (21H) address: 00100001. Value written into this register makes the sensor go into measurement mode with different settings.
4. Control register value: 00010001. This sets the sensor to do a single measurement in low power mode.
5. Measurement phase. When this gets over, ODINT pin it pulled down by the sensor and the chip is notified.
6. The sensor now has to read the measured data. For that, it first has to go into write mode to write the data register value on SDA. Hence, 00011000 again.
7. Data register (17H) address: 00010111. This stores 64 bit data: 1st 16 are status bits, next 16 are Z data, then Y and then X data. All data values are vectors with first bit being the sign bit.
8. Start condition for read operation.
9. Sensor address with read mode bit (1): 00011001. This allows values to be read from SDA by the chip.
10. 16 bits of status register. The last bit being 1 signifies that data is stored successfully from the measurement and is ready to be read.
11. 16 bits of Z field data.
12. 16 bits of Y field data.
13. 16 bits of X field data.
14. Stop condition.

**Figure 20.4.S3: Digital waveform on the SDA line is used to explain the Sensor Interface (SI) block architecture. The complete data flow is handled by SI, which generates the data to be written on SDA and reads from SDA through an I2C digital block in between. The data vectors (11, 12 and 13) are parsed by SI and sent to the backscatter modulator.**

**Additional References:**

[4] S. Guo et al., "An Efficiency-Enhanced CMOS Rectifier with Unbalanced-Biased Comparators for Transcutaneous-Powered High-Current Implants," *JSSC*, vol. 44, no. 6, pp. 1796-1804, 2009.

[5] X. Liu et al., "An 86% Efficiency 12 μW Self-Sustaining PV Energy Harvesting System With Hysteresis Regulation and Time-Domain MPPT for IOT Smart Nodes," *JSSC*, vol. 50, no. 6, pp. 1424-1437, 2015.

[6] Donghoon Son et al., "A 5-D Localization Method for a Magnetically Manipulated Untethered Robot using a 2-D Array of Hall-effect Sensors," *IEEE/ASME Transactions on Mechatronics*, vol. 21, no. 2, pp. 708-716, 2016.


978-1-7281-3205-1/20/$31.00 ©2020 IEEE